04,11

Phase composition, structure and transport characteristics of $ZrO_2-Sc_2O_3$ solid solution crystals additionally doped with Yb_2O_3

© M.A. Borik[1], G.M Korableva[1,2], A.V. Kulebyakin[1,¶], I.E. Kuritsyna[1,2], E.E. Lomonova[1], F.O. Milovich[1,3], V.A. Myzina[1], N.Yu. Tabachkova[1,3]

[1] Prokhorov General Physics Institute of the Russian Academy of Sciences
Moscow, Russia
[2] Osipyan Institute of Solid State Physics RAS
Chernogolovka, Russia
[3] National University of Science and Technology „MISiS“,
Moscow, Russia

[¶] E-mail: kulebyakin@lst.gpi.ru

Received July 8, 2021;
revised July 8, 2021;
accepted July 8, 2021

The effect of the co-doped Yb_2O_3 on the transport characteristics and stabilization of the cubic phase in solid solutions based on $ZrO_2-Sc_2O_3$ has been carried out. $(ZrO_2)_{1-x-y}(Sc_2O_3)_x(Yb_2O_3)_y$ solid solution crystals, where ($x = 0.07-0.09$; $y = 0.01-0.03$), were grown by directional crystallization of the melt in a cold crucible. It is shown that crystals with a cubic fluorite structure were obtained at a total concentration of stabilizing oxides Sc_2O_3 and Yb_2O_3 above 10 mol%. At a fixed concentration of Sc_2O_3, crystals with a total concentration of stabilizing oxides of 10 mol.%, which have the structure of a pseudocubic t''-phase, have the maximum conductivity. It is shown that an increase in the Yb_2O_3 concentration in the field of cubic solid solutions leads to a decrease in the conductivity of the crystals. The $(ZrO_2)_{0.9}(Sc_2O_3)_{0.09}(Yb_2O_3)_{0.01}$ crystals have the maximum conductivity in the entire temperature range.

Keywords: Crystal growth from melt, zirconium dioxide, solid electrolytes.

DOI: 10.21883/PSS.2022.13.52071.01s

1. Introduction

Materials based on zirconium dioxide (zirconia) stabilized with scandium oxide (scandia) feature high values of ionic conductivity and have the potential to be used as solid electrolytes in various electrochemical devices (e.g., solid oxide fuel cells [1–4], electrolysis units, and sensors [5–6]). Membranes made from scandia-stabilized zirconia provide an opportunity to reduce considerably the operating temperature of solid oxide fuel cells and thus prolong their service life.

Phase diagrams for the $ZrO_2-Sc_2O_3$ system were presented in [7–11], but the boundaries of phase existence differ from one study to the other and were determined only approximately. This is attributable to the existence of metastable phases in this system and, consequently, to the dependence of the phase composition on the synthesis technique and conditions. The structure and transport characteristics of $ZrO_2-(9-11$ mol.%) Sc_2O_3 solid solutions were investigated in [12–14]. It is shown that long-term high-temperature annealing of solid solutions based on ZrO_2 stabilized only by Sc_2O_3 can lead to a change in the phase composition and degradation of transport characteristics. Additional doping of solid solution with rare-earth oxides is one of the ways toward improving the properties of solid electrolytes based on $ZrO_2-Sc_2O_3$. This technique allows one to obtain stable cubic high-conductivity solid solutions. CeO_2 [15–17], Y_2O_3 [18,19], Gd_2O_3 [17,20], and Sm_2O_3 [17] are used as co-doping oxides. Specific co-doping oxides are chosen so as to obtain a single-phase cubic solid solution stable at temperatures ranging from room temperature to the operating one ($700-1000^\circ$C) and preserve the high conductivity values typical of $ZrO_2-Sc_2O_3$. Yb_2O_3 [17,20] is also an efficient co-doping oxide that stabilizes the high-conductivity cubic phase. The experimental data for $(ZrO_2)_{0.88}(Sc_2O_3)_{(0.12-x)}(Yb_2O_3)_x$ ($x = 0.0$; 0.01; 0.03; 0.05) synthesized by spark plasma sintering revealed that the composition with 1 mol.% Yb_2O_3 features the highest conductivity (8.3 mS/cm at 650°C) [21]. In [22], the highest conductivity (0.30 S/cm at 1000°C) was observed for single-phase cubic $(ZrO_2)_{0.91}(Sc_2O_3)_{0.08}(Yb_2O_3)_{0.01}$ samples produced by solid-state synthesis. The results of studies into the properties of materials based on scandia-stabilized zirconia co-doped with rare-earth oxides often differ even if the compositions are the same [23–29]. These discrepancies are attributable to the fact that the phase composition, the structure, and, consequently, the transport characteristics of solid solutions depend strongly on the synthesis technique and parameters. The use of single crystals in studies into the „composition–structure–transport characteristics“ interrelation alleviates the need for examining the effect of microstructure (grain size and relative density), which is another factor crucial for ceramic

Table 1. Compositions of grown crystals, their symbols, and their density

Chemical composition	Symbol	Density, g/cm^3
$(ZrO_2)_{0.92}(Sc_2O_3)_{0.07}(Yb_2O_3)_{0.01}$	7Sc1YbSZ	5.926 ± 0.001
$(ZrO_2)_{0.91}(Sc_2O_3)_{0.07}(Yb_2O_3)_{0.02}$	7Sc2YbSZ	5.989 ± 0.003
$(ZrO_2)_{0.90}(Sc_2O_3)_{0.07}(Yb_2O_3)_{0.03}$	7Sc3YbSZ	6.049 ± 0.003
$(ZrO_2)_{0.91}(Sc_2O_3)_{0.08}(Yb_2O_3)_{0.01}$	8Sc1YbSZ	5.925 ± 0.006
$(ZrO_2)_{0.90}(Sc_2O_3)_{0.08}(Yb_2O_3)_{0.02}$	8Sc2YbSZ	5.969 ± 0.002
$(ZrO_2)_{0.89}(Sc_2O_3)_{0.08}(Yb_2O_3)_{0.03}$	8Sc3YbSZ	6.007 ± 0.002
$(ZrO_2)_{0.90}(Sc_2O_3)_{0.09}(Yb_2O_3)_{0.01}$	9Sc1YbSZ	5.863 ± 0.003
$(ZrO_2)_{0.89}(Sc_2O_3)_{0.09}(Yb_2O_3)_{0.02}$	9Sc2YbSZ	5.918 ± 0.003
$(ZrO_2)_{0.88}(Sc_2O_3)_{0.09}(Yb_2O_3)_{0.03}$	9Sc3YbSZ	5.980 ± 0.002

materials, on the electrophysical properties. In ceramic materials, these factors exert a considerable influence on the ratio between the conductivity of the grain bulk and the grain-boundary conductivity [30–35]. In the present study, materials were synthesized by directional crystallization of the melt in a cold crucible [36]. This method was used earlier to synthesize crystals of a wide range of solid electrolytes [37–40].

The aim of the study is to examine the effect of additional doping with Yb_2O_3 on the phase composition, the structure, and the transport characteristics of $ZrO_2-Sc_2O_3$ solid solution crystals.

2. Experimental part

Single crystals of solid solutions were grown by directional crystallization of the melt in a cold container 130 mm in diameter with direct high-frequency heating (5.28 MHz, Kristall-407 setup). The crystal growth rate was 10 mm/h.

The density of single crystals was determined by hydrostatic weighing.

A JEOL 5910 LV scanning election microscope fitted with an INCA energy dispersive spectroscopy module was used to examine the distribution of scandium and ytterbium oxides throughout the length of crystals. Point-by-point measurements were performed along the crystal growth axis.

The phase composition of the grown crystals was studied by X-ray diffractometry (with a Bruker D8 diffractometer) and by Raman spectroscopy. A laser with a wavelength of 532 nm served as the excitation source for Raman studies of the phase composition.

The structure of crystals was examined by transmission electron microscopy (TEM) with the use of a JEM-2100 microscope at an accelerating voltage of 200 kV.

The transport characteristics of crystals were studied by impedance spectroscopy in a temperature interval of 450–900°C at frequencies ranging from 1 Hz to 5 MHz.

3. Results and discussion

Crystals of $(ZrO_2)_{1-x-y}(Sc_2O_3)_x(Yb_2O_3)_y$ ($x = 0.07-0.09$; $y = 0.01-0.03$) solid solutions were grown by directional crystallization of the melt in a cold crucible. The crystals were columnar, which is typical of this growth technique. Their length and cross-section dimensions were $\sim 30-40$ mm and $10-20$ mm, respectively. The compositions of crystals, their symbols, and their density are listed in Table 1. At a fixed concentration of Sc_2O_3, the density of crystals increases with the concentration of Yb_2O_3 in the solid solution.

Only the 7Sc1YbSZ, 7Sc2YbSZ, and 8Sc1YbSZ crystals were opaque with strong light scattering throughout their entire volume. Other compositions from the studied range produced homogeneous transparent crystals. This is

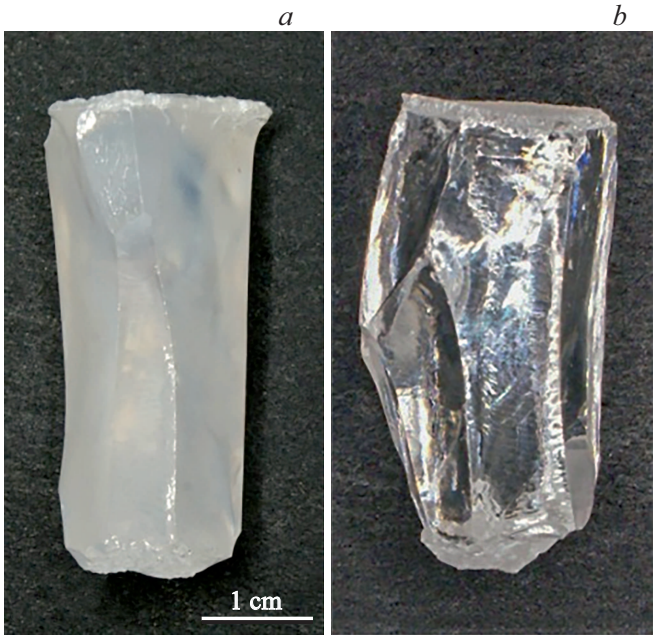

Figure 1. Appearance of the 8Sc1YbSZ (*a*) and 9Sc1YbSZ (*b*) crystals.

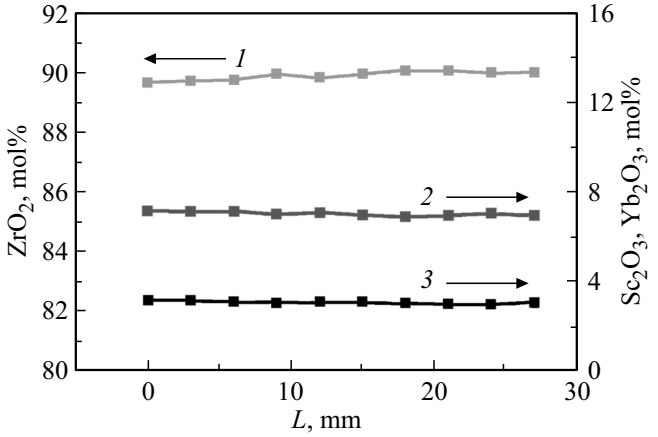

Figure 2. Distribution of zirconium (*1*), scandium (*2*), and ytterbium (*3*) oxides throughout the length of the 7Sc3YbSZ crystal.

illustrated by Fig. 1, which presents the appearance of the 8Sc1YbSZ and 9Sc1YbSZ crystals.

Thus, homogeneous transparent single crystals were obtained when the overall concentration of stabilizing oxides Sc_2O_3 and Yb_2O_3 was ≥ 10 mol.%.

Analysis of the distribution of scandium and ytterbium oxides throughout the length of crystals revealed that all the examined samples are homogeneous in composition and that the concentration of Sc_2O_3 and Yb_2O_3 is almost the same as their concentration in the initial charge. Sc^{3+} and Yb^{3+} were introduced into the composition of crystals uniformly throughout their entire length without any significant variations in the process of growth. Fig. 2 presents the distribution of scandium, ytterbium, and zirconium oxides in the 7Sc3YbSZ crystal.

The results of phase analysis based on X-ray diffractometry (XRD) data demonstrated that the 7Sc1YbSZ, 7Sc2YbSZ, and 8Sc1YbSZ crystals contained only tetragonal ZrO_2. The other crystals were single-phase with a cubic fluorite structure. The phase composition and lattice parameters of the studied crystals are presented in Table 2.

Table 2. Phase composition and lattice parameters of crystals

Sample	Phase composition*	Lattice parameters	
		a, nm	c, nm
7Sc1YbSZ	t'	0.3598(1)	0.5119(1)
7Sc2YbSZ	t'	0.3602(1)	0.5116(1)
7Sc3YbSZ	c	0.5102(1)	
8Sc1YbSZ	t'	0.3598(1)	0.5113(1)
8Sc2YbSZ	c	0.5099(1)	
8Sc3YbSZ	c	0.5098(1)	
9Sc1YbSZ	c	0.5094(1)	
9Sc2YbSZ	c	0.5096(1)	
9Sc3YbSZ	c	0.5097(1)	

Note. * t', c — denote tetragonal and cubic ZrO_2, respectively.

The phase composition and lattice parameters of crystals doped with 7 mol.% Sc_2O_3 and doped additionally with Yb_2O_3 varied with the Yb_2O_3 concentration. The 7Sc1YbSZ crystals contained only tetragonal phase t' with tetragonality $c/\sqrt{2}a = 1.006$. Lattice parameter a grew as the concentration of Yb_2O_3 increased to 2 mol.%, while lattice parameter c decreased under the same conditions. Tetragonality $c/\sqrt{2}a = 1.004$ in the 7Sc2YbSZ crystals is lower than that in 7Sc1YbSZ. When the concentration of Yb_2O_3 increases to 3 mol.% in the 7Sc3YbSZ crystals,

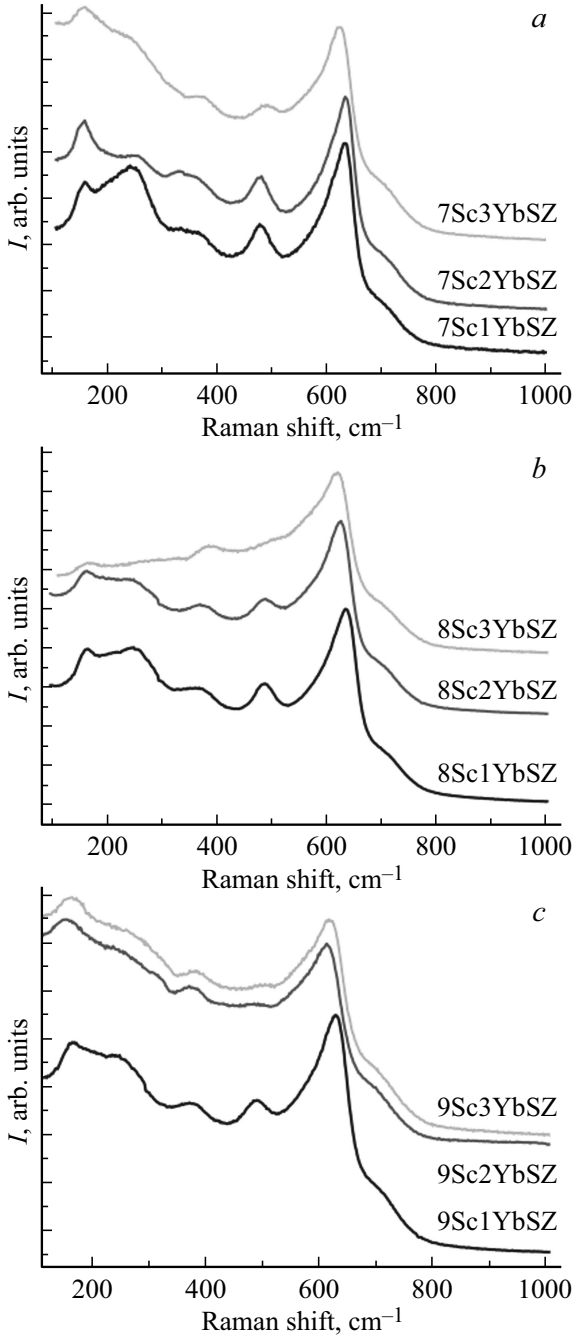

Figure 3. Raman spectra of the 7ScxYbSZ (*a*), 8ScxYbSZ (*b*), and 9ScxYbSZ (*c*) crystals.

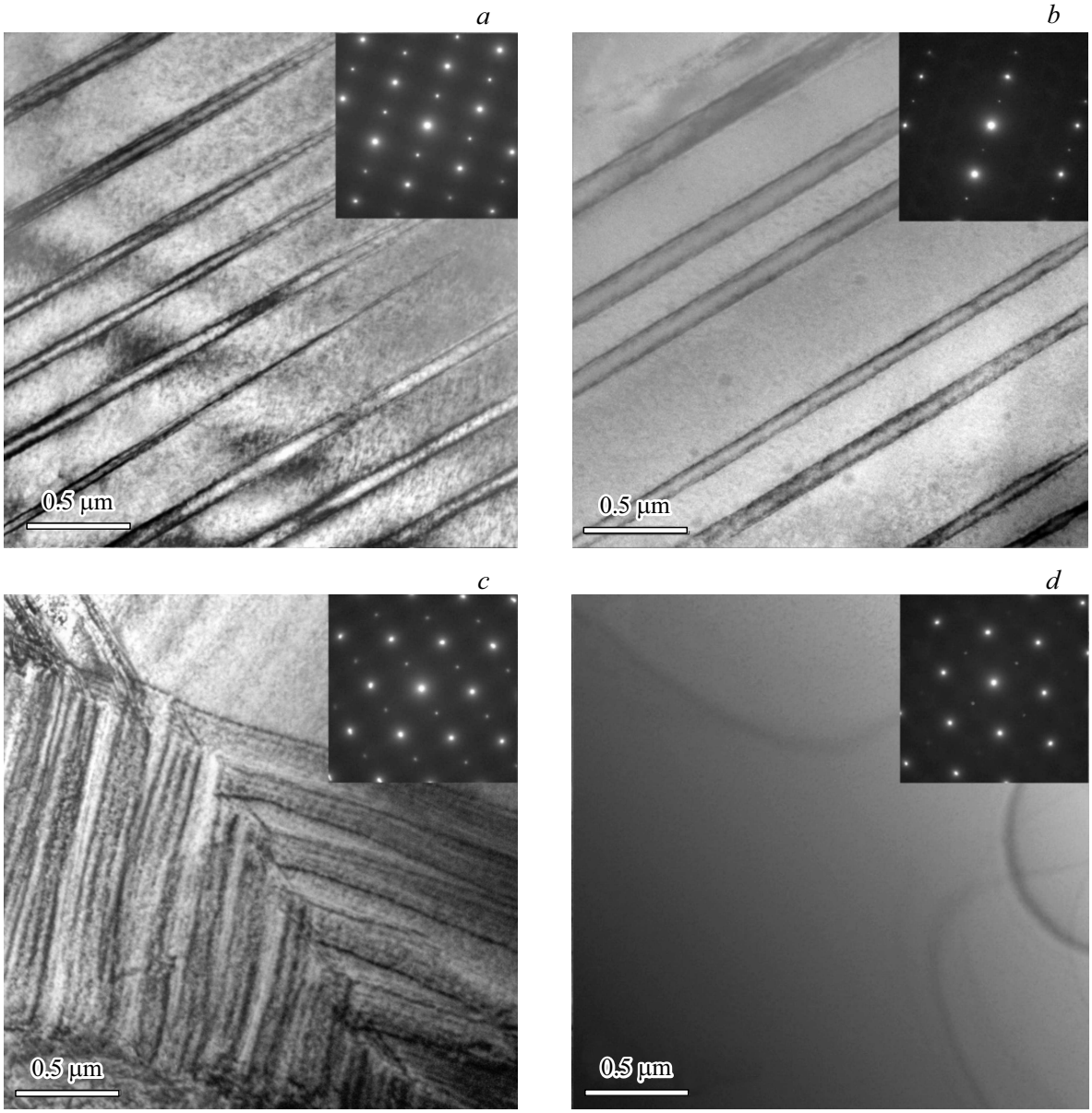

Figure 4. Images of the structure of the 7Sc1YbSZ (*a*), 7Sc2YbSZ (*b*), 8Sc1YbSZ (*c*), and 8Sc2YbSZ (*d*) crystals. Electron diffraction patterns corresponding to these regions are shown in the insets.

the cubic phase stabilizes throughout the entire crystal volume.

Of all the crystals doped with 8 mol.% of Sc_2O_3, only the ones doped additionally with 1 mol.% of Yb_2O_3 were tetragonal (tetragonality $c/\sqrt{2}a = 1.005$). The 8Sc2YbSZ and 8Sc3YbSZ crystals were single-phase cubic.

When the concentration of Sc_2O_3 in solid solutions was 9 mol.%, all the crystals in the studied range of compositions were cubic. The lattice parameter in the cubic region of compositions increased with the Yb_2O_3 concentration.

Thus, in the studied range of compositions, crystals with a cubic fluorite structure were synthesized when the overall concentration of stabilizing oxides Sc_2O_3 and Yb_2O_3 was ≥ 10 mol.%.

The phase composition of crystals was also examined by Raman spectroscopy (Fig. 3). Raman spectra of the 7Sc1YbSZ, 7Sc2YbSZ, and 8Sc1YbSZ crystals are typical of tetragonal ZrO_2 [41]. Raman spectra of other crystals are typical of either the cubic structure of zirconia [42] or tetragonal t''-phase [43]. t''-phase has tetragonality $c/\sqrt{2}a = 1$, but belongs to space group of symmetry $P4_2/nmc$ due to a slight displacement of oxygen atoms in the anion sublattice. It follows from the analysis of the Raman spectra that the 8Sc3YbSZ, 9Sc2YbSZ, 9Sc3YbSZ crystals have a cubic structure, while the 7Sc3YbSZ, 8Sc2YbSZ, 9Sc1YbSZ crystals have a t''-phase structure, which is the boundary between the tetragonal and cubic phases.

Thus, the results of Raman spectroscopy confirm the XRD data, while also providing an opportunity to distinguish single-phase crystals with a cubic structure from the ones with the closely similar t''-phase structure.

TEM studies of the structure of crystals based on ZrO_2 solid solutions stabilized with Sc_2O_3 and Yb_2O_3 oxides revealed that the 7Sc1YbSZ, 7Sc2YbSZ, and 8Sc1YbSZ crystals contained twins (Fig. 4). Twinning is associated with the release of elastic stresses accumulated in the phase transition of the cubic phase into the tetragonal one occurring when crystals are cooled in the process of growth.

The electron diffraction patterns of the 7Sc1YbSZ, 7Sc2YbSZ, and 8Sc1YbSZ crystals demonstrated that they contained tetragonal zirconia. Twin-free regions were not found in these crystals. Twins in 7Sc2YbSZ were larger than the ones in the 7Sc1YbSZ and 8Sc1YbSZ crystals.

TEM data reveal no visible defects (dislocations, dislocation loops, twins, etc.) in the 8Sc2YbSZ crystals (Fig. 4, *d*). The obtained images corresponded to the structure typical of cubic low-defect single crystals. At the same time, diffraction patterns contained reflections that are forbidden for a cubic lattice and allowed for a tetragonal structure. The presence of (110) and (100) reflections is indicative of ordered displacement of oxygen atoms and, by extension, violation of the symmetry typical of space group Fm3m. The structure and features of electron diffraction patterns for the 7Sc3YbSZ and 9Sc1YbSZ crystals were similar to the structure of 8Sc2YbSZ. Thus, it follows from the comparison of XRD, Raman, and TEM data on the phase composition that homogeneous and transparent 7Sc3YbSZ, 8Sc2YbSZ, and 9Sc1YbSZ single crystals have the t''-phase structure. The electron diffraction patterns for 8Sc3YbSZ, 9Sc2YbSZ, and 9Sc3YbSZ demonstrated that these crystals belong to the cubic ZrO_2 phase.

Fig. 5 shows the dependence of the conductivity of crystals on the Yb_2O_3 content. The conductivity of crystals containing 7 mol.% Sc_2O_3 increases with the concentration of Yb_2O_3 in the solid solution. The conductivity of the 7Sc3YbSZ crystals is the highest. The conductivity of crystals containing 8 mol.% Sc_2O_3 varies nonmonotonically with the concentration of Yb_2O_3 and features a well-pronounced maximum corresponding to 8Sc2YbSZ. The conductivity of crystals containing 9 mol.% Sc_2O_3 decreases as the concentration of Yb_2O_3 grows. Thus, at a fixed concentration of Sc_2O_3, the crystals with an overall concentration of stabilizing oxides of 10 mol.% (specifically, 7Sc3YbSZ, 8Sc2YbSZ, and 9Sc1YbSZ) have the highest conductivity. Aside from that, the conductivity of crystals increases with the Sc_2O_3 content: the 9Sc1YbSZ crystals have higher conductivity values than 8Sc2YbSZ and 7Sc3YbSZ.

The observed concentration dependences of conductivity are easy to interpret if one takes into account the data on the phase composition of samples and the crystal structure. When the Yb_2O_3 content increases from 1 to 3 mol.% in crystals with 7 mol.% Sc_2O_3, their tetragonality decreases

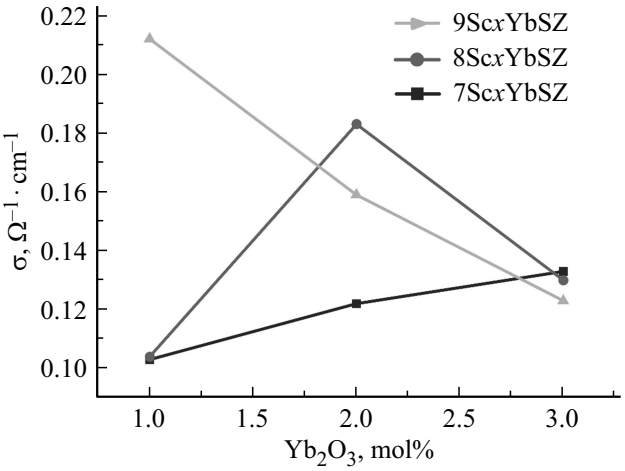

Figure 5. Variation of the ionic conductivity of crystals at a temperature of 900°C with the Yb_2O_3 content.

and the phase composition changes from tetragonal t' to the t''-phase. At the same time, twins were observed in the 7Sc1YbSZ and 7Sc2YbSZ crystals containing t'-phase. The size of twins increased with the Yb_2O_3 concentration. No visible defects were found in the 7Sc3YbSZ crystals containing t''-phase. Thus, the additional introduction of Yb_2O_3 into crystals containing 7 mol.% Sc_2O_3 leads to a change in the phase composition, a decrease in the number of defects, and an increase in the conductivity of the crystals. The 7Sc3YbSZ single crystals containing t''-phase had the maximum conductivity.

The conductivity of the 8Sc2YbSZ crystals with a structure of the pseudo-cubic t''-phase is higher than that of the tetragonal 8Sc1YbSZ crystals containing twins. When the concentration of Yb_2O_3 increases to 3 mol.%, the cubic phase stabilizes and the conductivity of the 8Sc3YbSZ crystals decreases.

The 9Sc1YbSZ crystals with the t''-phase structure have the highest conductivity in the group of solid solutions containing 9 mol.% Sc_2O_3. An increase in the concentration of Yb_2O_3 results in stabilization of the cubic phase in the 9Sc2YbSZ and 9Sc3YbSZ crystals and causes a reduction in the conductivity values.

Thus, single crystals with the structure of pseudo-cubic t'' phase (with oxygen atoms displaced from high-symmetry positions typical of the cubic phase) and an overall concentration of stabilizing Sc_2O_3 and Yb_2O_3 oxides of 10 mol.% have the highest conductivity within the studied range of compositions.

4. Conclusion

The phase composition and the transport characteristics of $(ZrO_2)_{1-x-y}(Sc_2O_3)_x(Yb_2O_3)_y$ solid solutions crystals ($x = 0.07-0.09$; $y = 0.01-0.03$) grown by directional crystallization of the melt in a cold container were studied.

It was demonstrated that the pseudo-cubic t''-phase stabilizes at an overall concentration of stabilizing Sc_2O_3 and Yb_2O_3 oxides of 10 mol.%. In contrast to tetragonal crystals containing t'-phase, single crystals with the structure of pseudo-cubic t''-phase contain no twins.

At a fixed concentration of Sc_2O_3, the crystals with an overall concentration of stabilizing oxides of 10 mol.% (specifically, 7Sc3YbSZ, 8Sc2YbSZ, and 9Sc1YbSZ, which have the structure of pseudo-cubic t''-phase) have the highest conductivity. It was demonstrated that the conductivity of crystals decreases when the concentration of Yb_2O_3 increases in the region of cubic solid solutions. The 9Sc1YbSZ crystals have the highest conductivity of all the studied compositions.

Funding

This study was supported by a grant from the Russian Science Foundation (project No. 19-72-10113). Equipment provided by the „Materials Science and Metallurgy“ Common Use Center was used in structural studies, which were supported financially by the Ministry of Science and Higher Education of the Russian Federation (13.CKP.21.0033).

Conflict of interest

The authors declare that they have no conflict of interest.

References

[1] S.P.S. Badwal, F.T. Ciacchi, D. Milosevic. Solid State Ionics **136–137**, 91 (2000).
[2] J.W. Fergus. J. Power Sources **162**, 30 (2006).
[3] J. Fergus. J. Minerals, Met. Mater. Soc. **59**, 56 (2007).
[4] S.C. Singhal, K. Kendall. High Temperature Solid Oxide Fuel Cells: Fundamentals, Design, and Applications. Elsevier Science Ltd., Oxford (2003). P. 387–389.
[5] V.V. Kharton, F.M.B. Marques, A. Atkinson. Solid State Ionics **174**, 135 (2004).
[6] M. Morales, M. Segarra. Materials Issues for Solid Oxide Fuel Cells Design. Handbook of Clean Energy Systems. John Wiley & Sons, Ltd. (2015). P. 1–15.
[7] R. Ruh, H.J. Garrett, R.F. Domagala, V.A. Patel. J. Am. Ceram. Soc. **60**, *9*, 400 (1977).
[8] M. Yashima, M. Kakihana, M. Yoshimura. Solid State Ionics **86–88**, 1131 (1996).
[9] T.-S. Sheu, J. Xu, T.-Y. Tien. J. Am. Ceram. Soc. **76**, *8*, 2027 (1993).
[10] H. Fujimori, M. Yashima, M. Kakihana, M. Yoshimura. J. Am. Ceram. Soc. **81**, 2885 (1998).
[11] H. Fujimori, M. Yashima, M. Kakihana, M. Yoshimura. J. Appl. Phys. **91**, 6493 (2002).
[12] W. Araki, T. Koshikawa, A. Yamaji, T. Adachi. Solid State Ionics **180**, 1484 (2009).
[13] O. Yamamoto, Y. Arai, Y. Takeda, N. Imanishi, Y. Mizutani, M. Kawai, Y. Nakamura. Solid State Ionics **79**, 137 (1995).
[14] K. Nomura, Y. Mizutani, M. Kawai, Y. Nakamura, O. Yamamoto. Solid State Ionics **132**, 235 (2000).
[15] K. Du, C.-H. Kim, A.H. Heuer, R. Goettler, Z. Liu. J. Am. Ceram. Soc. **91**, 1626 (2008).
[16] D.A. Agarkov, M.A. Borik, S.I. Bredikhin, I.N. Burmistrov, G.M. Eliseeva, V.A. Kolotygin, A.V. Kulebyakin, I.E. Kuritsyna, E.E. Lomonova, F.O. Milovich, V.A. Myzina, P.A. Ryabochkina, N.Yu. Tabachkova, T.V. Volkova. J. Materiomics **5**, 273 (2019).
[17] H.A. Abbas, C. Argirusis, M. Kilo, H.-D. Wiemhöfer, F.F. Hammad, Z.M. Hanafi. Solid State Ionics **184**, *1*, 6 (2011).
[18] S. Omar, W.B. Najib, W. Chen, N. Bonanos. J. Am. Ceram. Soc. **95**, 1965 (2012).
[19] M.A. Borik, S.I. Bredikhin, V.T. Bublik, A.V. Kulebyakin, I.E. Kuritsyna, E.E. Lomonova, F.O. Milovich, V.A. Myzina, V.V. Osiko, P.A. Ryabochkina, S.V. Seryakov, N.Yu. Tabachkova. J. Cryst. Growth **457**, 122 (2017).
[20] V.V. Lakshmi, R. Bauri. Solid State Sci. **13**, 1520 (2011).
[21] V. Shukla, A. Kumar, I.L. Basheer, K. Balani, A. Subramaniam, S. Omar. J. Am. Ceram. Soc. **100**, 204 (2017).
[22] A. Yamaji, T. Koshikawa, W. Araki, T. Adachi. J. Eng. Mater. Technol. **131**, 011010 (2008).
[23] A. Spirin, V. Ivanov, A. Nikonov, A. Lipilin, S. Paranin, V. Khrustov, A. Spirina. Solid State Ionics **225**, 448 (2012).
[24] A. Kumar, A. Jaiswal, M. Sanbui, S. Omar. J. Am. Ceram. Soc. **100**, *2*, 659 (2017).
[25] S. Terauchi, H. Takizawa, T. Endo, S. Uchida, T. Terui, M. Shimada. Mater. Lett. **23**, 273 (1995).
[26] D.-S. Lee, W. Kim, S. Choi, J. Kim, H.-W. Lee, J.-H. Lee. Solid State Ionics **176**, 33 (2005).
[27] Z. Wang, M. Cheng, Z. Bi, Y. Dong, H. Zhang, J. Zhang, Z. Feng, C. Li. Mater. Lett. **59**, 2579 (2005).
[28] S.T. Norberg, S. Hull, I. Ahmed, S.G. Eriksson, D. Marrocchelli, P.A. Madden, P. Li, J.T.S. Irvine. Chem. Mater. **23**, *6*, 1356 (2011).
[29] J.T.S. Irvine, J.W.L. Dobson, T. Politova, S.G. Martin, A. Shenouda. Faraday Discussions **134**, 41 (2006).
[30] V.V. Osiko, M.A. Borik, E.E. Lomonova, Synthesis of refractory materials by skull melting. In: Springer hand book of crystal growth. Springer, N.Y. (2010). P. 433–477.
[31] X.J. Chen, K.A. Khor, S.H. Chan, L.G. Yu. Mater. Sci. Eng. A **335**, *1–2*, 246 (2002).
[32] M. Hirano, S. Watanabe, E. Kato. J. Am. Ceram. Soc. **82**, *10*, 2861 (1999).
[33] A. Cheikh, A. Madani, A. Touati, H. Boussetta, C. Monty. J. Eur. Ceram. Soc. **21**, 1837 (2001).
[34] M. Aoki, Y.-M. Chiang, I. Kosacki, L.J.-R. Lee, H. Tuller, Y. Liu. J. Am. Ceram. Soc. **79**, 1169 (1996).
[35] S. Shukla, S. Seal, R. Vij, S. Bandyopadhyay. NanoLetters **3**, *3*, 397 (2003).
[36] P. Mondal, A. Klein, W. Jaegermann, H. Hahn. Solid State Ionics **118**, 331 (1999).
[37] S. Berendts, M. Lerch. J. Cryst. Growth. **371**, 28 (2013).
[38] I. Valov, V. Ruhrup, R. Klein, T.-C. Rödel, A. Stork, S. Berendts, M. Dogan, H.-D. Wiemhöfer, M. Lerch, J. Janek. Solid State Ionics. **180**, 1463 (2009).

[39] J.-P. Eufinger, M. Daniels, K. Schmale, S. Berendts, G. Ulbrich, M. Lerch, H.-D. Wiemhöfer, J. Janek. Phys. Chem. Chem. Phys. **46**, 25583 (2014).
[40] M.A. Borik, S.I. Bredikhin, V.T. Bublik, A.V. Kulebyakin, I.E. Kuritsyna, E.E. Lomonova, F.O. Milovich, V.A. Myzina, V.V. Osiko, P.A. Ryabochkina, N.Yu. Tabachkova. J. Am. Ceram. Soc. **100**, *12*, 5536 (2017).
[41] M. Borik, G. Korableva, A. Kulebyakin, I. Kuritsyna, N. Larina, E. Lomonova, F. Milovich, V. Myzina, P. Ryabochkina, N. Sidorova, N. Tabachkova, T. Volkova. Crystals **11**, *2*, 83 (2021).
[42] H. Fujimori, M. Yashima, M. Kakihana, M. Yoshimura. J. Am. Ceram. Soc. **81**, *11*, 2885 (1998).
[43] Y. Hemberger, N. Wichtner, C. Berthold, K.G. Nickel. Int. J. Appl. Ceram. Technol. **13**, *1*, 116 (2016).